Andi Trimulyono
Haikal Atthariq
Deddy Chrismianto
Samuel Samuel

http://dx.doi.org/10.21278/brod73203

ISSN 0007-215X
eISSN 1845-5859

INVESTIGATION OF SLOSHING IN THE PRISMATIC TANK WITH VERTICAL AND T-SHAPE BAFFLES

UDC 532.5:532.58:532.594
Original scientific paper

Summary

The demand for liquid carriers, such as liquefied natural gas (LNG), has increased in recent years. One of the most common types of LNG carriers is the membrane type, which is often built by a shipyard with a prismatic tank shape. This carrier is commonly known for its effective ways to mitigate sloshing using a baffle. Therefore, this study was performed to evaluate sloshing in a prismatic tank using vertical and T-shape baffles. The sloshing was conducted with 25% and 50% filling ratios because it deals with the nonlinear free-surface flow. Furthermore, the smoothed particle hydrodynamics (SPH) was used to overcome sloshing with ratio of a baffle and water depth is 0.9. A comparison was made for the dynamic pressure with the experiment. The results show that SPH has an acceptable accuracy for dynamic and hydrostatic pressures. Baffle installation significantly decreases the wave height, dynamic pressure and hydrodynamic force.

Keywords: *Smoothed particle hydrodynamics; Sloshing; Vertical baffle; T-shape baffle; Dynamic Pressure; Wave height; Hydrodynamic force*

1. Introduction

The capacity of liquid carriers has increased in recent years, and this is caused by the increasing demand for liquefied Natural Gas (LNG). A common type is the membrane type, which is often built by a shipyard, and is shaped like a prismatic tank. One of the advantages of the membrane-type carrier is that its shape is similar to a ship hull and has a large capacity. A naturally occurring phenomenon in LNG carriers is sloshing, defined as the movement of fluid due to the excitation force in the tank, which is effectively mitigated using a baffle. Sloshing is a nonlinear phenomenon that is difficult to be overcome in fluid dynamics. Several preliminary studies have been performed, including experimental and numerical analyses, which have been made popular by the rapid advancement of computer technology in recent years. An overview of sloshing with hydro-structure interactions was performed with a direct calculation approach [1]. Evaluation of the added resistance coupled with sloshing was performed using the potential flow theory [2]. This study employed a numerical approach to analyze sloshing using smoothed particle hydrodynamics (SPH). SPH is a meshless and purely Lagrangian approach used to

reproduce large deformation and nonlinear phenomena. In this study, weakly compressible SPH (WCSPH) is used to reproduce sloshing in the prismatic tank.

Initially, SPH was used to solve astrophysical problems [3]. However, Monaghan developed SPH for free surface flow for dam-break and water wave cases [4]. Moreover, it is widely applied and used for structural interactions between waves with breakwaters [5]. With an experimental validation, SPH was applied in a long-distance water propagation that occured in a large wave basin [6]. Furthermore, to reduce the reflections in a numerical wave tank (NWT), an active wave absorption was developed [7]. This was combined with open boundaries and used to conduct a water wave simulation [8]. The implementation of SPH for NWT with incompressible SPH (ISPH) was performed using GPU to reduce pressure noise in WCSPH scheme [9]. Therefore, SPH is used to solve the water wave and has good accuracy for free surface flow.

The SPH application in violent flow sloshing, which usually occurs with respect to a low filling ratio due to an obstacle in the rectangular tank, was carried out in one-phase SPH [10]. Furthermore, one- and two-phase SPH were used in a prismatic tank with a low-pass filter technique to reduce pressure oscillation due to the nature of WCSPH [11]. These were studied in a three-dimensional (3D) domain [12], and the results showed that the SPH had good accuracy and also highly a computational cost. A preliminary study was conducted using elastic baffle to reduce sloshing in the rectangular tank [13]. A two-dimensional analysis study was also performed using a T-shape baffle to reduce the effect of this phenomenon in a RANS solver [14]. SPH coupled with the smoothed finite element method was used to investigate the impact of sloshing in a rectangular tank with a flexible vertical and T-shape baffle [15]. The long-duration simulation of this phenomenon in rectangular-, pill-, spherical- and cylindrical-shaped tanks had been studied in a three-dimensional domain [16]. The implementation of δ-SPH and particle shifting with flexible baffle and elastic walls of the rectangular tank were used to tackle sloshing [17]. A comparison study was performed using volume of fluid (VOF), SPH, and arbitrary Lagrangian-Eulerian to analyze the braking and roll responses of partly filled tank vehicles [18]. Preliminary research was performed on single and double vertical baffles in rectangular tanks [19].

This study used single-, and double-vertical and T-shape baffles to investigate sloshing in a prismatic tank. Its heights were based on previous research [19], and the ratio of the baffles to water depth is relatively 0.75 to 0.9. The selected baffle height in this study was 0.9. A pressure sensor was used to verify the validity of SPH simulation based on experimental research carried out by Trimulyono et al. [20]. Moreover, two water heights were set to capture free surface deformation inside the tank. Its oscillatory motion has 25% and 50% filling ratios. DualSPHysics version 5.0, an open-source SPH solver, was used to simulate sloshing in the prismatic tank [21]. DualSPHysics was implemented using general purpose computing on graphics processing units (GPGPU) [22]. It ensures a million particles are handled using a single GPU. Moreover, the advanced visualization was performed using Blender version 2.92.

Sloshing in the prismatic tank was used in a single-phase SPH, and the results revealed that the vertical baffle has a significant effect, such as reducing fluid movements and hydrodynamic pressure. Finally, hydrodynamic force and moment decreased.

2. Theoretical background and method

2.1 Experimental setup of sloshing and SPH simulation.

Figure 1 shows the experimental setup of sloshing in the prismatic tank, involving three pressure sensors [20]. However, only one of them was used to validate SPH simulation, and

only two filling ratios, i.e., 25% and 50%, were used (Figure 1). The pressure sensor located in the bottom was used to validate the SPH results. As a consequence, the 25% filling ratio was situated near a free surface, whereas that of the 50% was located in the mid-water depth. This is one of the reasons why pressure sensors located at the bottom were used to validate SPH result. Reproducing the pressure caused by sloshing was also challenging, especially when the 25% filling ratio was used. Four cameras were used to capture free surface deformation, which was equally installed inside and outside the oscillation machine. The detailed information of the sloshing experiment is stated in Ref. [20].

Figure 2 shows the geometry of the prismatic tank for SPH computation, where L, H, *l*, and *d* are its length, height, width, and water depth, respectively. Table 1 and Figure 3 show the tank's dimension and the three types of baffle shapes with the 25% filling ratio. The baffle height and water depth ratio were 0.9, and the vertical one was positioned in the middle of the tank. Meanwhile, the distance of the double baffle was equivalent to the tank's width, which was divided into three sections. The T-shape baffle was set in the middle of the tank, and its width is ¼*l*, where *l* is also equivalent to width. Its thickness was set as 6.0 mm, and *d1* and *d2* are water the depths in the 25% and 50% filling ratios, respectively.

Figure 4 shows the displacement of the tank in the experiment based on the constant oscillatory rolling motion. In this study, its movement was directly imposed from the experiment (Figure 4). A roll motion is one of the dangerous movements in the seakeeping area; so it was considered in the present study. Sloshing tends to endanger a ship when it is energetic, especially when the excitation frequency is near or identical to the natural frequency of the tank.

The amplitude of the roll motion is 8.66^0 with sloshing excitation frequencies of 1.04 and 1.30 Hz for the 25% and 50% filling ratios, respectively. The findings shows that the excitation frequency is close to the natural frequency of the prismatic tank [20].

Table 1. Principal dimensions of prismatic tank

Dimension	(m)
L	0.38
L	0.30
H	0.21
D	0.0525 (25%)
	0.1050 (50%)

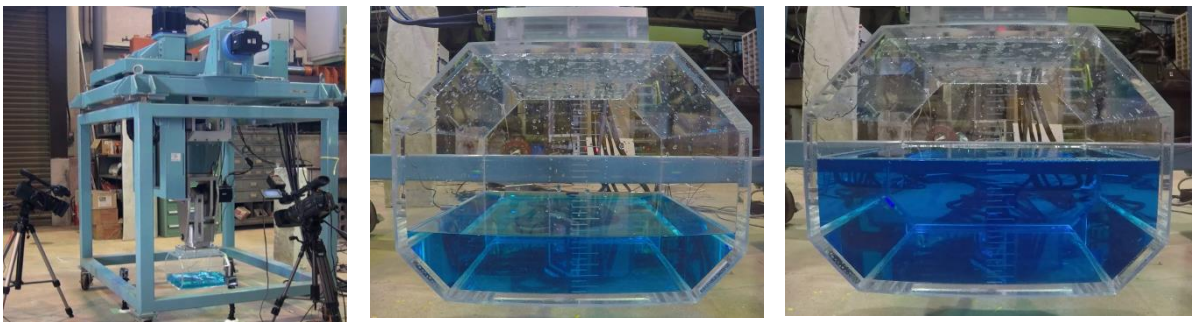

Fig. 1 Experimental condition of the sloshing filling ratio of 25% (a), condition of the water depth with filling ratios of 25% (b), and 50% (c) [20].

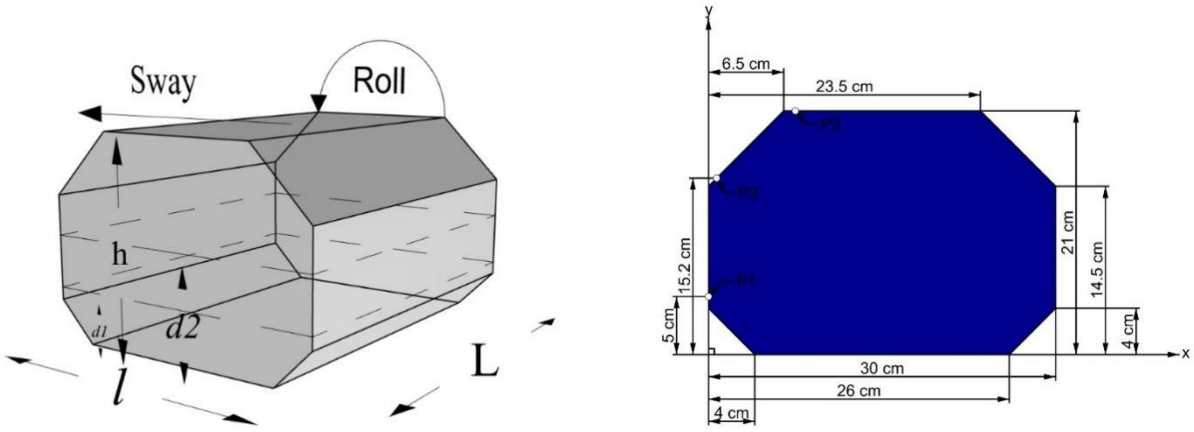

Fig. 2 Sketch of a prismatic tank with the principal dimension (a) and pressure sensor location (b).

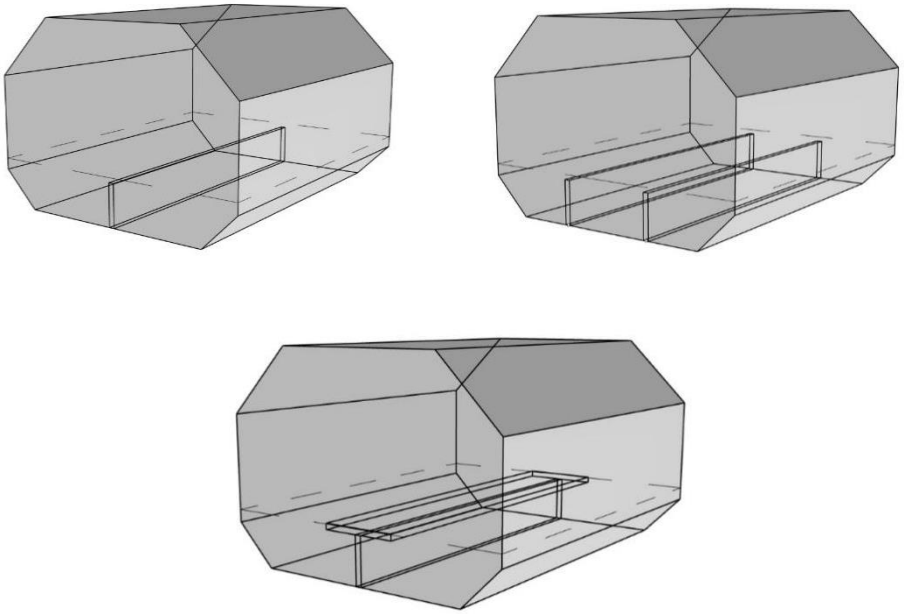

Fig. 3 Sketch of the prismatic tank with a single-vertical baffle (a) double-vertical baffle (b) and T-shape baffle (c).

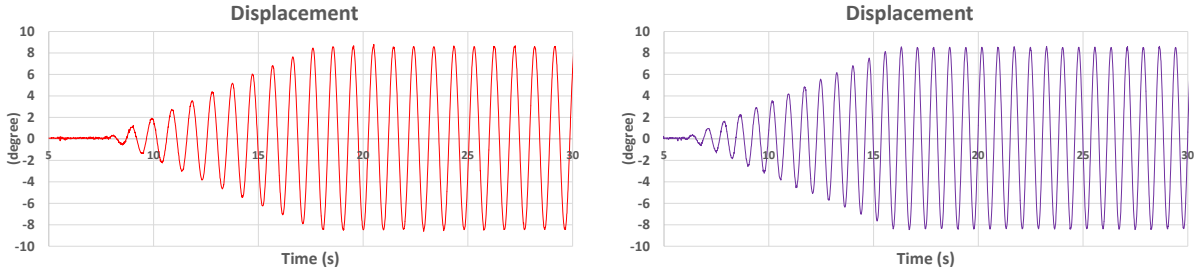

Fig. 4 Displacement of the prismatic tank in the SPH computation with filling ratio 25% (a) and 50% (b)

2.2 Smoothed particle hydrodynamics.

Smoothed particle hydrodynamics (SPH) was initially used in the astrophysical field developed by Monaghan [3] and Lucy [23]. Later on, It was applied to the free surface flow for dam breaks and water waves on the beach [4]. SPH is a meshless and pure Lagrangian approach that involves using an interpolation scheme to approximate the physical values and derivatives of a continuous field using discrete evaluation points. These are identified as smoothed particles with mass, velocity, and position. The quantities are obtained as a weighted average from adjacent particles within the smoothing length (h) to reduce the range of contribution from the neighboring ones. The main features of the SPH method, based on integral interpolants, are described in detail in Ref. [24] and [25].

Figure 5 shows the radius of particle a in the kernel function, and its contribution is weighed using the smoothing length, where $\boldsymbol{r_{ab}}$ is the distance between particles a and b and W_{ab} is the kernel function. In SPH, the field function $\boldsymbol{A}(\boldsymbol{r})$ in domain Ω is integrally approximated as Eq (1), where W and $\boldsymbol{r}$ are the kernel function and position of the vector, respectively.

Eq (1) is approximated into a discrete form by replacing the integral aspect with a summation of the neighboring particles regarding the compact support of particle a at spatial position $\boldsymbol{r}$, thereby leading to particle approximation in Eq (2). In this study, the Wendland kernel function was used in all simulations, where α_D is equal to $21/164\pi h^3$ in 3D, q is the nondimensional distance between particles a and b represented as r/h in Eq (3).

Eq (4) is the continuity equation with the delta-SPH term to reduce spurious pressure in SPH [26]. Eq (5) is the momentum equation in the SPH framework, where **g** is gravity due to acceleration, P_a and P_b are pressures in particles a and b. Π_{ab} is the artificial viscosity term, $\mu_{ab} = \frac{hv_{ab}.r_a}{r_{ab}^2+0.01h^2}$, $v_{ab} = v_a - v_b$ are vector velocities, $\overline{c_{ab}} = 0.5(c_a + c_b)$ is the mean speed of sound, and α is a coefficient that needs to be tuned to acquire proper dissipation.

DualSPHysics is based on WCSPH, to measure the pressure in WCSPH, an equation of state was used based on Eq (6), where c_o , ρ_0, and γ are the speed of sound at the reference density, and polytrophic constant, respectively. This equation is stiff, and a slight change in the density causes pressure fluctuation. This is one of the reasons why there is a pressure oscillation in WCSPH. Eq (7) is used to calculate the time step based on Monaghan's work, where Δt_f is based on the force per unit mass ($|f_a|$) while Δt_{cv} combines the Courant and the viscous time step controls, where CFL is a coefficient within the range of $0.1 \leq CFL \leq 0.3$.

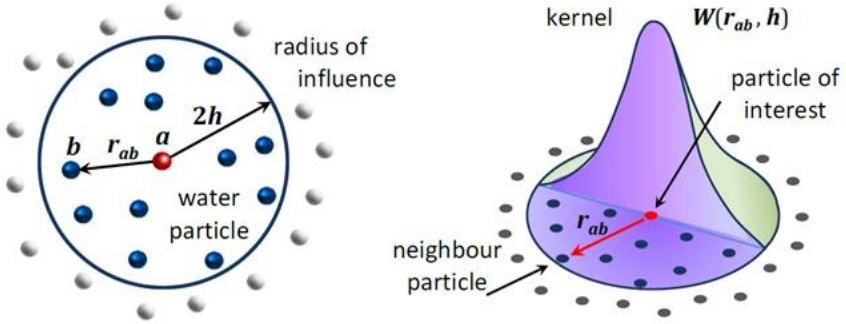

Fig. 5 Radius of the smoothing length and kernel function in SPH [27].

$$A(\boldsymbol{r}) = \int_{\Omega} A(\boldsymbol{r}) W(\boldsymbol{r} - \boldsymbol{r}', h)\, d\boldsymbol{r} \tag{1}$$

$$A(\boldsymbol{r}_a) \approx \sum_b A(\boldsymbol{r}_b) W(\boldsymbol{r}_a - \boldsymbol{r}_b, h) \frac{m_b}{\rho_b} \tag{2}$$

$$W(q) = \alpha_D \left(1 - \frac{q}{2}\right)^4 (2q+1) \quad 0 \le q \le 2 \tag{3}$$

$$\frac{d\rho_a}{dt} = \sum_b m_b \boldsymbol{v}_{ab} \cdot \nabla_a W_{ab} + 2\delta_\Phi h c_0 \sum_b (\rho_{b-} \rho_a) \frac{\boldsymbol{r}_{ab} \cdot \nabla_a W_{ab}}{\boldsymbol{r}_{ab}^2} \frac{m_b}{\rho_b} \tag{4}$$

$$\frac{d\boldsymbol{v}_a}{dt} = -\sum_b m_b \left(\frac{P_{a+P_b}}{\rho_a \cdot \rho_b} + \Pi_{ab}\right) \nabla_a W_{ab} + \mathbf{g} \tag{5}$$

$$where\ \Pi_{ab} = \begin{cases} \dfrac{-\alpha \overline{c_{ab}} \mu_{ab}}{\overline{\rho_{ab}}} & \boldsymbol{v}_{ab} \cdot \boldsymbol{r}_{ab} < 0 \\ 0 & \boldsymbol{v}_{ab} \cdot \boldsymbol{r}_{ab} > 0 \end{cases}$$

$$P = \frac{c_0^2 \rho_0}{\gamma} \left[\left(\frac{\rho}{\rho_0}\right)^\gamma - 1\right] \tag{6}$$

$$\Delta t_f = CFL \cdot min\left(\Delta t_f, \Delta t_{cv}\right) \tag{7}$$

$$\Delta t_f = min\left(\sqrt{\frac{h}{|\boldsymbol{f}_a|}}\right)$$

$$\Delta t_{cv} = min \frac{h}{c_s + max\left|\frac{h v_{ab} \cdot r_{ab}}{\left(r_{ab}^2 + \eta^2\right)}\right|}$$

Table 2 shows the parameters setup in SPH computation. In addition, the Wendland kernel function was applied in all computations using the symplectic timestep algorithm. The artificial viscosity term with α of 0.01 was used to obtain a proper dissipation. According to Trimulyono et al. [20], the speed of sound has a significant impact on the magnitude of pressure. A coefsound of 60 was used to reproduce similar accuracy on the pressure field. Coefh is the coefficient used to calculate smoothing length. In 3D, Coefh was defined as $Coefh = \frac{h}{dp\sqrt{3}}$. CFL is the coefficient used to obtain the Courant-Friedrichs-Lewy condition with 0.2 used for all computation. Delta-SPH was employed to reduce pressure oscillation, with a default value of 0.1 used in all computations. Dynamic boundary particles (DBPs) were adopted based on Crespo et al. [28]. DBPs are boundary particles that satisfy the same equations as fluid particles, but they are not moved by their forces. Instead, they either remain in a fixed position or move according to an imposed or assigned motion function. This includes the movement of objects, such as gates, wavemakers, or floating objects. When a fluid particle approaches a boundary, and the distance between its particles and that of the fluid is smaller than twice the smoothing length (h), the density of the affected boundary particles increases, leading to a pressure rise. The simulation time was set at 28 s due to the regular motion, which is the same with that after reaching a steady-state condition (Figure 4).

Table 2. Parameter setup of the SPH computation.

Parameters	
Kernel function	Wendland
Time step algorithm	Symplectic
Artificial viscosity coefficient (α)	0.01
Confound	60
Particle spacing (mm)	1.6
Coefh	1.2
CFL	0.2
Delta-SPH (δ_φ)	0.1
Simulation time (s)	28

3. Results and discussion

3.1 Hydrostatic and hydrodynamic pressures.

Figure 6 shows the hydrostatic pressure in the 50% filling ratio with and without a T-shape baffle. Based on Trimulyono research et al. [20], hydrostatic pressure was properly reproduced by SPH with a difference of 3%, as shown in Figure 6. Moreover, the hydrostatic pressure gradient is similar to an analytic solution where the pressure is the highest at the bottom and lowest on the free surface. Figure 7 depicts the dynamic pressure of sloshing with and without baffle configuration at t = 14.0 s. The free surface was violently deformed as compared to the use of baffle. The vertical baffle reduces the fluid movement by dampening through this instrument. T-shape baffle does the same by separating the fluid on each side, which also affects the water depth, thereby reducing the free surface deformation.

Figure 8 shows the dynamic pressure detected by a pressure sensor at the bottom of the tank (see Figure 2). The static pressure was subtracted from the hydrostatic pressure, thereby resulting in dynamic pressure. No significant pressure phase existed between SPH and experiment, which depicts that they have a similar velocity and displacement. Moreover, timing of the sensors used to capture dynamic pressure is similar. Hence certain properties such as fluid kinematics has similar tendencies as physics.

The hydrodynamic pressure consists of static and dynamic pressures. Figure 8(a) shows the impact of the hydrodynamic pressure on the 25% filling ratio, with the red and purple lines depicting an experiment, and SPH without a baffle, respectively. The green, yellow, and black lines are dynamic pressure with single-, double-, and T-shape baffles. Figure 8(b) shows the comparison of the average and peak pressures between SPH and experiment. The difference in the peak and average pressure is 4.6 % and 4.8 %. The first magnitude is referred to as the dynamic pressure, which is gradually reduced, as shown in Figure 7. The second is dynamic pressure resulting from the movement of fluid to the top of the tank. Its magnitude is lesser than first the dynamic pressure because it is affected by the fluid movement without any sudden acceleration. In the sloshing phenomena, dynamic or impact pressure has to be minimized to avoid structural damages or explosions from dangerous liquid cargoes such as LNG.

One of the effective ways to mitigate sloshing is the use of a vertical baffle. Ma et al. reported that the vertical baffles effectively reduce sloshing in a rectangular tank [19]. A similar

outcome was obtained using a prismatic tank with a T-shape baffle. The results show that fluid movements inside the tank were significantly reduced causing a decrease in the pressure magnitude. Using one vertical baffle reduced the pressure by 85.80%, whereas the use of two vertical baffles effectively decreased the pressure by 88.24%. The T-shape baffle efficiently reduced the pressure by 82.60%.

Figure 9(a) shows the dynamic pressure of the 50% filling ratio and accuracy, which is slightly different from those of the 25% filling ratio. Figure 9(b) indicates that the peak pressure could not be captured by SPH and made the average pressure accuracy lower than that of the 25% filling ratio. However, the trend of the dynamic pressure is similar after the peak pressure. Although SPH could not capture the peak pressure, the timing accuracy of the pressure sensor was similar to those of the experiment and 25% filling ratio. The findings revealed that the dynamic pressure was reproduced by SPH, although the accuracy was slightly reduced as compared to that of the 25% filling ratio. The single-vertical baffle reduced the pressure by 94.5%, whereas the double-vertical baffles decreased the pressure by 91.2%. The T-shape baffle effectively reduced the pressure by 91.0%.

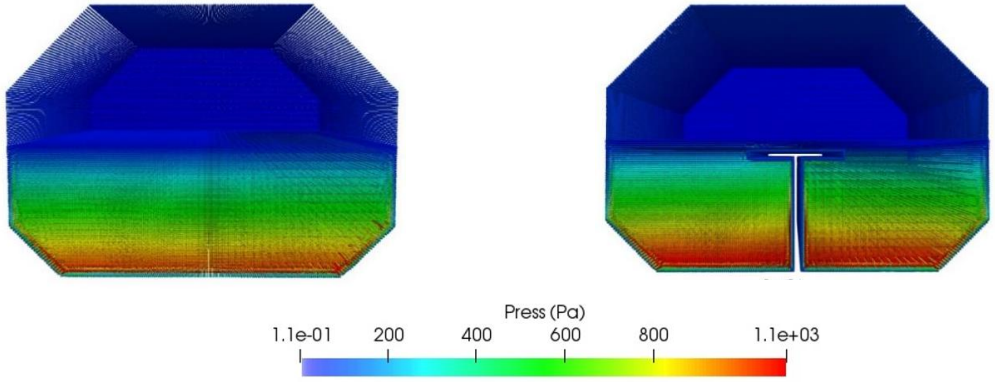

Fig. 6 Hydrostatic pressure in the 50% filling ratio without and with T -shaped baffle.

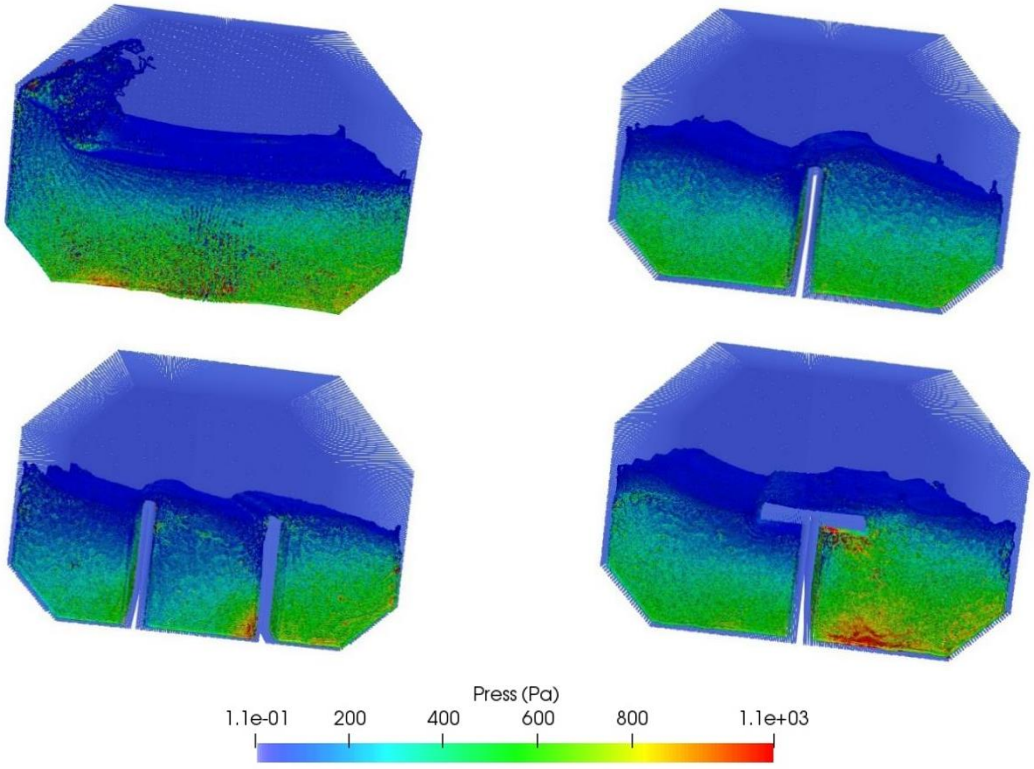

Fig. 7 Comparison of dynamic pressure in the 50% filling ratio with t = 14.0 s

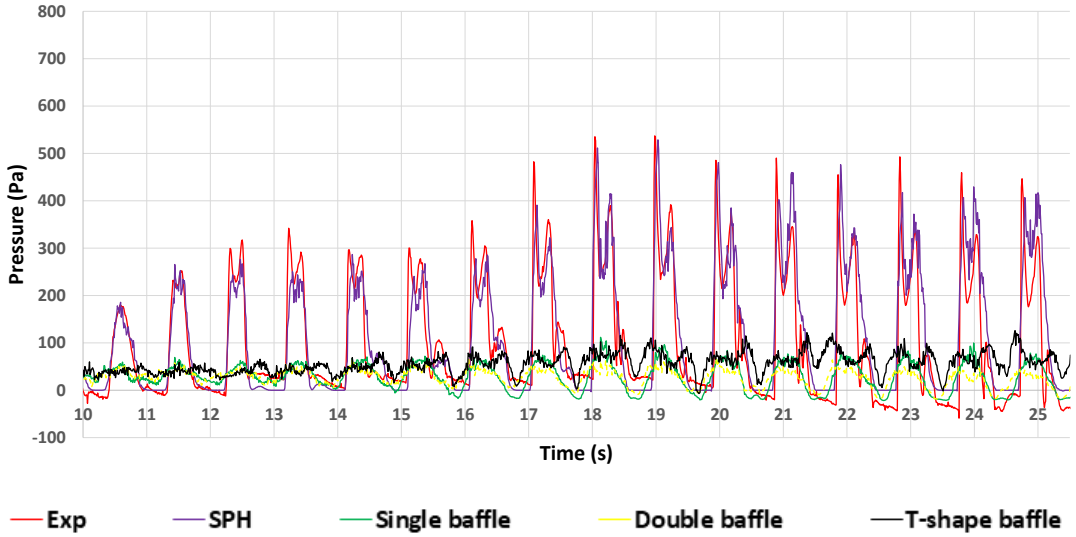

(a)

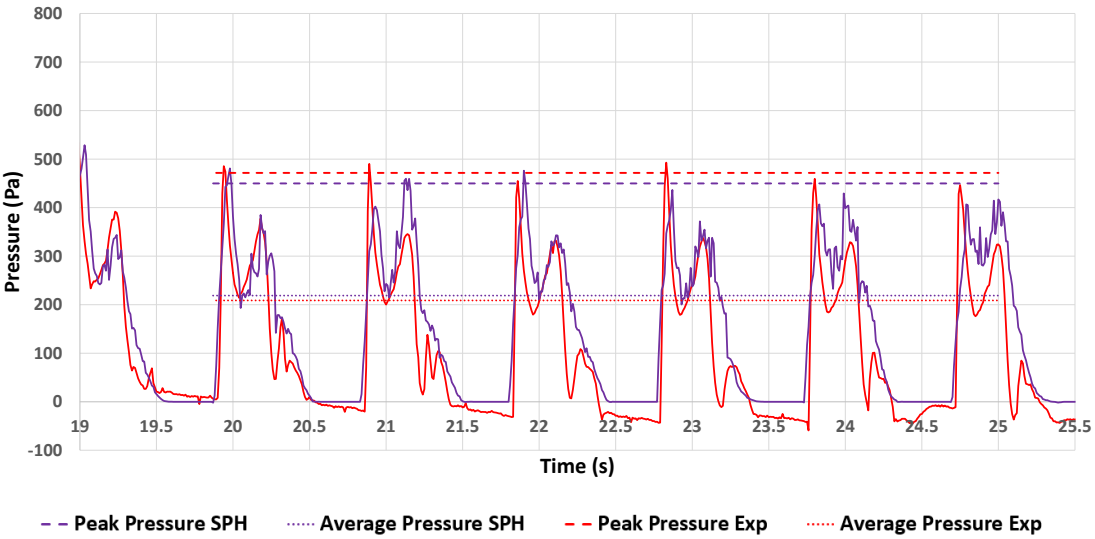

(b)

Fig. 8 Comparison of the dynamic pressure with and without baffles for the 25% filling ratio (a) and the difference in the dynamic pressure for the average and peak pressures (b).

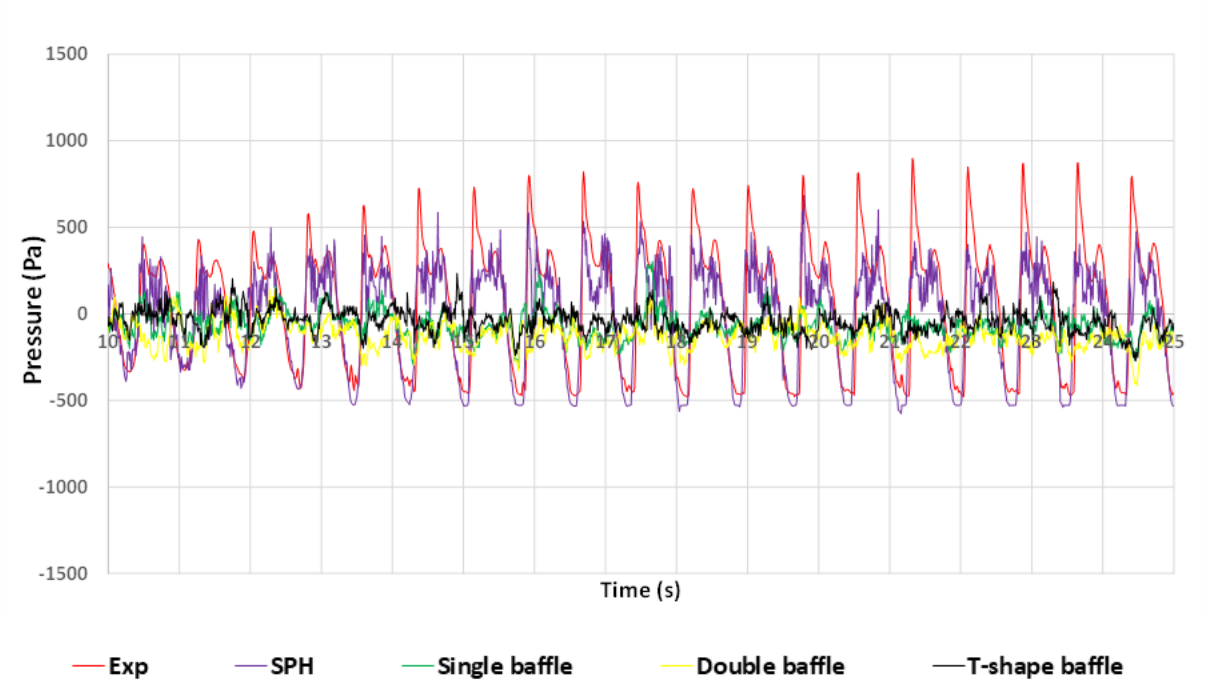

(a)

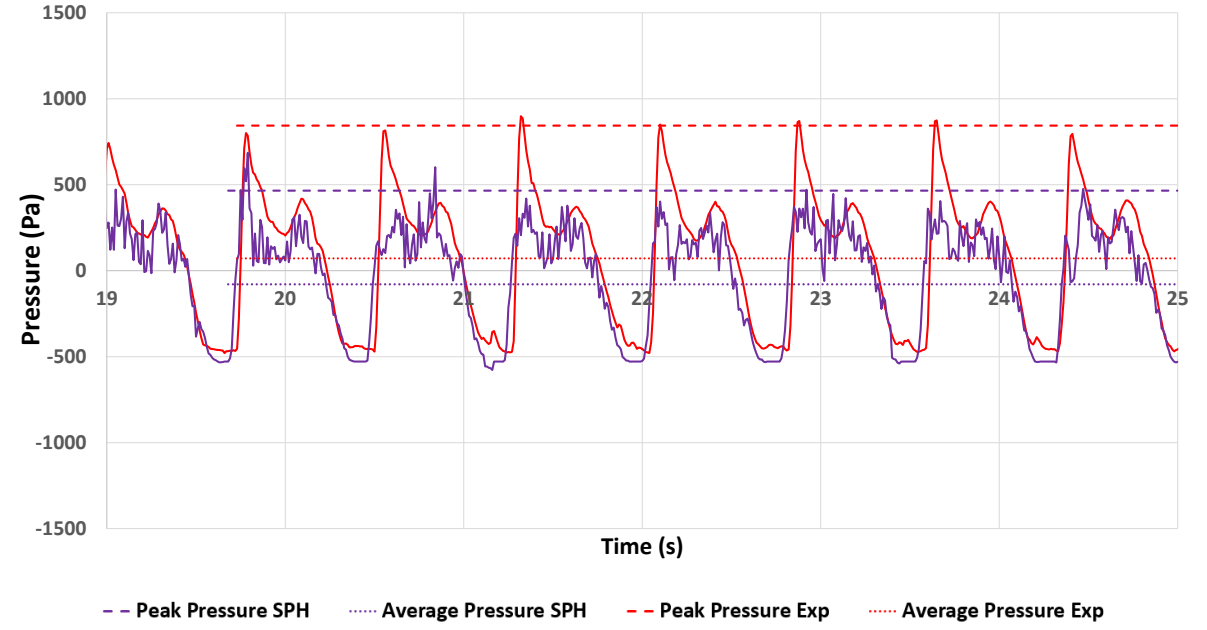

(b)

Fig. 9 Comparison of the dynamic pressure with and without baffles for the 50% filling ratio (a) and the difference of the dynamic pressure for the average and peak pressures (b).

3.2 Free surface deformation

An advanced visualization process was conducted using the open-source Blender version 2.92, which was freely downloaded at https://www.blender.org/. Furthermore, with the present technique, the post-processing of SPH became more attractive and similar to physics. Figure 10 depicts the comparison of visualized particles and advanced surface texturing using Blender [29]. Figure 10 shows that the fluid looks like real fluid and is more attractive as compared with

the particle form. The post-processing of advanced texturing was performed for all simulations using the GPU.

The free surface deformation in the tank was influenced by the excitation force. The existence of energetic sloshing in fluid movements is usually chaotic and complicated. It tends to exist when the frequency of the excitation force is close to the natural frequency of the tank. To effectively mitigate fluid movements, the use of baffles is recommended. Figures 11 and 12 show that the fluid run-up reaches the tank top without baffle installation. In contrast, after the installation of baffles it became calm.

The use of a single-vertical baffle suppress the wave height by approximately 86.3%. Moreover, it reduces the dynamic pressure, as shown in Figure 11. The fluid becomes calm because the dynamic pressure triggered by the fluid-accelerated movement is suppressed. Similar results were obtained using double-vertical and T-shape baffles. The double-vertical and T-shape baffles suppress the wave height by relatively 91.7% and 95.0%, respectively. Based on a visual observation, the use of a vertical baffle caused the fluid to be damped, and it also underwent suction after passing through the baffle. The vertical baffle suppressed the kinetic energy, thereby causing the fluid movement to become slower than that without its installation. The T-shape baffle showed similar phenomena, and the fluid became calm because was damped. This condition is based on the fact that the fluid movement was suppressed when it passed through the baffle. The fluid became calm due to a sudden change in the water depth, especially when it passes the T-shape baffle, thereby suppressing the height. Figure 12 shows that it is lesser when compared with that without baffle installation.

In the 50% filling ratio, the use of a single vertical baffle suppressed the wave height by approximately 79.0%. The 25% filling ratio exhibited similar tendency phenomena. The vertical baffle dampened the fluid movement because it experienced a suction effect after passing through it, thereby reducing the wave height and ensuring calmness. The double-vertical baffle suppressed the wave height by approximately 95.0%. Therefore, a high result was obtained using this equipment because it was suppressed twice. The height near the tank was affected by its movement, which is lesser compared with that without a baffle. The dynamic pressure was reduced, and the fluid became calm. The T-shape baffle was used to suppress the wave height by relatively 79.0%. In the 50% filling ratio, the T-shape baffle produced a lesser damped fluid than that in the 25% filling ratio. Therefore, when the fluid was suctioned, the water depth closer to the wall increased the wave height, as shown in Figure 12. Future research can be performed on the effect of the T–shaped baffle width on sloshing.

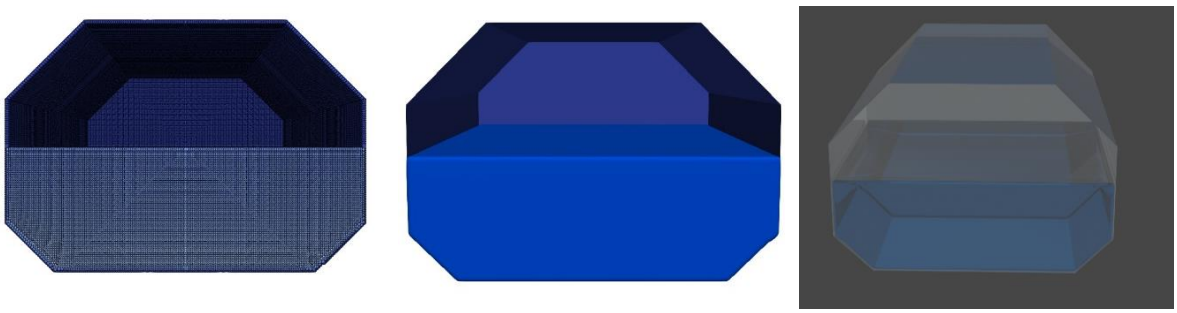

Fig. 10 Visualizations of the particle, iso-surface, and surface texture.

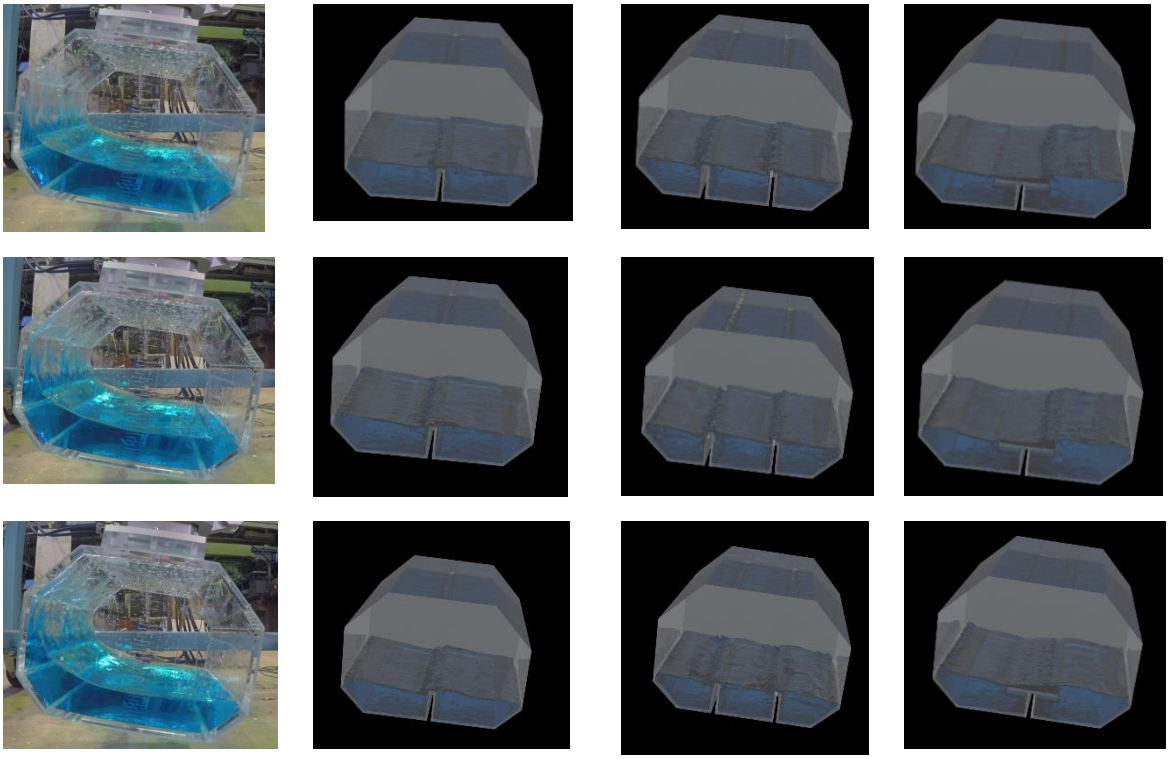

Fig. 11 Comparison of the free surface deformations inside a tank with and without baffles in the 25% filling ratio.

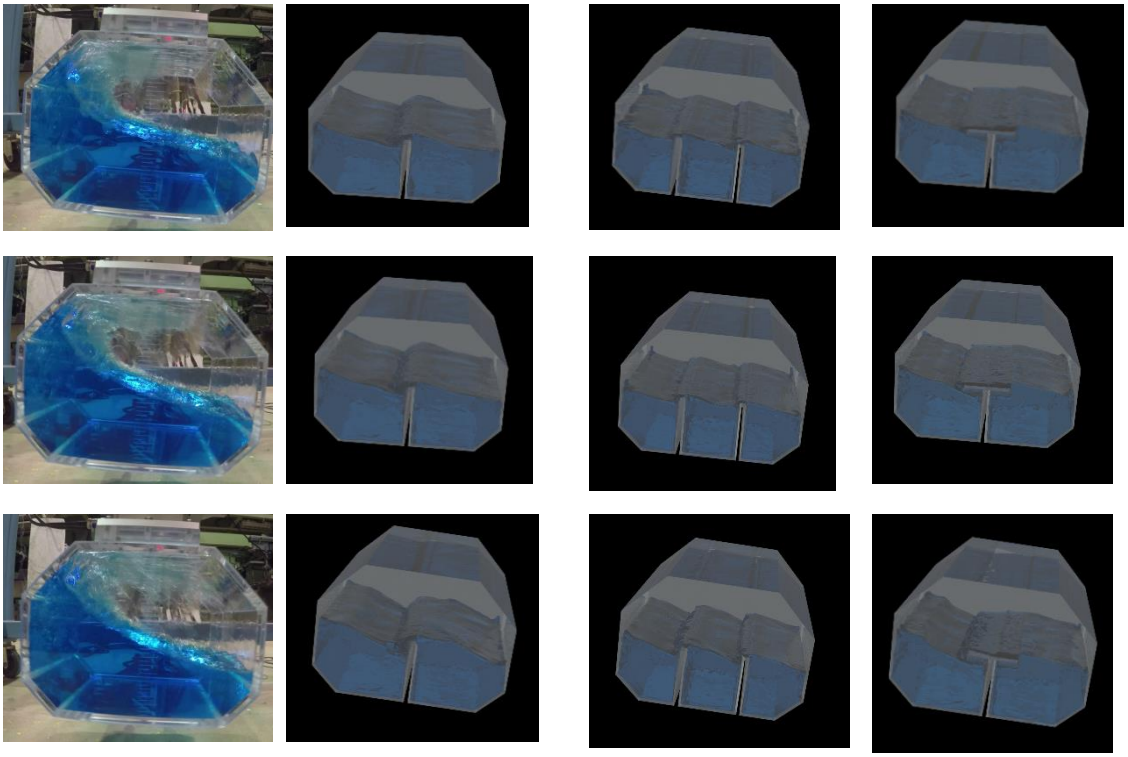

Fig. 12 Comparison of the free surface deformations inside a tank with and without baffles in the 50% filling ratio.

3.3 Hydrodynamic force

The sloshing experiment was conducted with a forced oscillation machine in 4 degrees of freedom [20]. The instrument performed both regular and irregular motions. Coupled motions, such as roll and heave, were utilized during the sloshing experiment. This research used only regular motions to reproduce the sloshing phenomenon. Because of the baffle effect is evident in regular and irregular motions.

Hydrodynamic force exists because the fluid inside the tank was forced to move by an oscillation machine. Figure 13 shows the impact of the hydrodynamic force on the 25% filling ratio. The red line represents hydrodynamic force without baffles, and the green, yellow, and black lines represent the use of single-, double-, and T-shape baffles, respectively. The hydrodynamic force without a baffle is higher than that with the installation with a slight difference, unlike the dynamic pressure or wave height. The hydrodynamic force in the tank was caused by constant forced oscillation during the sloshing period. As a result, the difference tends to be minor compared with the dynamic pressure, assuming the motion is forced oscillation. The difference between hydrodynamic force without and with a single- vertical baffle is relatively 33%. A similar trend involving double and T-shape baffles shows that the difference is 35% and 47%, respectively. The T-shape baffle was effectively used to reduce the hydrodynamic force and the force acting in the middle of the tank, which is caused by its shape.

The 50% filling ratio showed that the hydrodynamic force have a similar trend, as shown in Figure 14. The single- and double-vertical baffles effectively reduced the hydrodynamic force by 30%, whereas the T-shape reduced it by 49%. Hence, the use of baffles could be an alternative to reduce sloshing in the prismatic tanks. Furthermore, sloshing is a forced motion, sloshing induced by external force excitation needs to be investigated in the future.

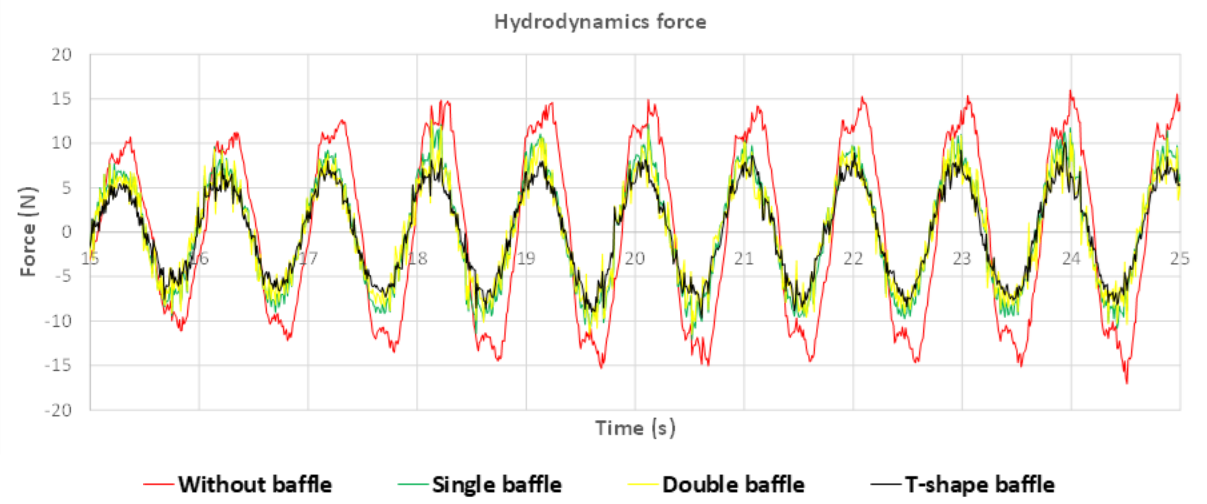

Fig. 13 Hydrodynamic force due to sloshing in the 25% filling ratio with and without baffles.

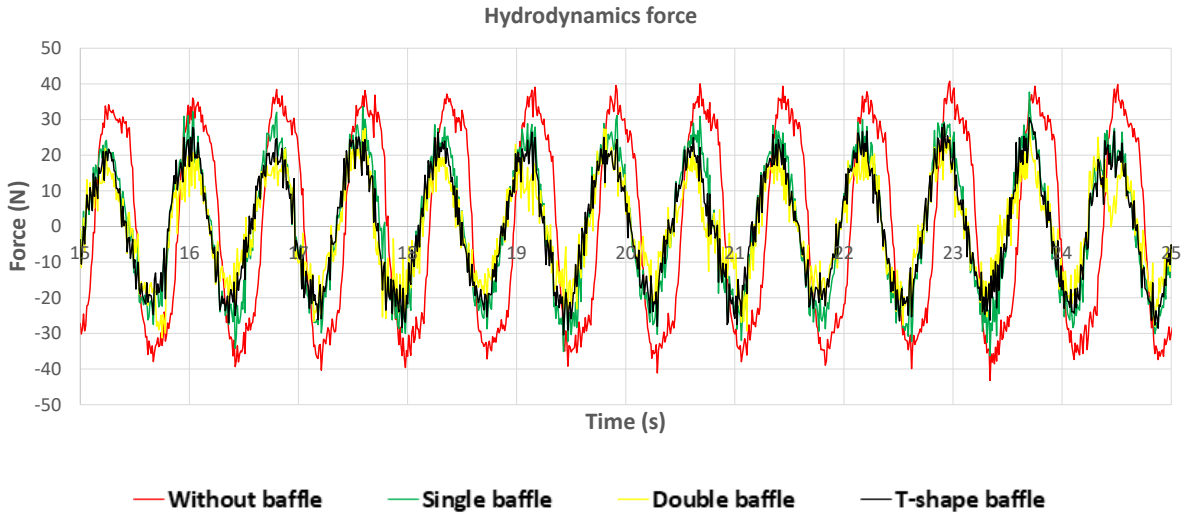

Fig. 14 Hydrodynamics force due to sloshing in filling ratio 50% with and without baffle.

4. Conclusions

The sloshing simulation in the prismatic tank was successfully conducted in two filling ratios. It was reproduced with SPH, one of the promising methods. The results prove that single- and double-vertical and T-shape baffles can be effectively used to mitigate sloshing in a prismatic tank. The results also reveal that they efficiently reduced the impact pressure caused by energetic sloshing. The wave height shows the linear effect as the dynamic pressure, which was reduced by the single- and double-vertical, and T-shape baffles. Hydrodynamic force was slightly decreased by these baffles, although the excitation force exhibited an oscillatory motion. Nonetheless, future research needs to be conducted to determine the effect of sloshing on coupled or ship motions.

Acknowledgments

The authors are grateful to Dr. Yuuki Taniguchi and Prof. Hirotada Hashimoto (Osaka Prefecture University) for the experimental data used to conduct this research. The authors appreciate the ship hydrodynamics laboratory for providing computer facilities. We want to thank LPPM Universitas Diponegoro for providing professional English proofreading.

REFERENCES

[1] Malenica, Š., Kwon. S. H., 2012. An overview of the hydro-structure interactions during sloshing impacts in the tanks of LNG carriers. *Brodogradnja*, 64, 22 – 30.

[2] Martić, I., Degiuli. N., Ćatipović, I., 2017. Evaluation of the added resistance and ship motions coupled with sloshing using potential flow theory. *Brodogradnja*. 67, 109 – 122. https://doi.org/10.21278/brod67408

[3] Gingold, R.A., Monaghan, J.J., 1977. Smoothed particle hydrodynamics: theory and application to non-spherical stars. *Monthly Notices of the Royal Astronomical Society*, 181, 375–389. https://doi.org/10.1093/mnras/181.3.375

[4] Monaghan, J.J., 1994. Simulating free surface flows with SPH. *Journal Computational Physics*, 110, 399–406. https://doi.org/10.1006/jcph.1994.1034

[5] Zhang, F., Crespo, A., Altomare, C., Domínguez, J., Marzeddu, A., Shang, S.P., Gómez-Gesteira, M., 2018. Dualsphysics: A numerical tool to simulate real breakwaters. *Journal of Hydrodynamics*, 30, 95–105. https://doi.org/10.1007/s42241-018-0010-0

[6] Trimulyono, A., Hashimoto, H., 2019. Experimental Validation of Smoothed Particle Hydrodynamics on Generation and Propagation of Water Waves. *Journal of Marine Science and Engineering*, 7, 17. https://doi.org/10.3390/jmse7010017
[7] Altomare, C., Domínguez, J.M., Crespo, A.J.C., González-Cao, J., Suzuki, T., Gómez-Gesteira, M., Troch, P., 2017. Long-crested wave generation and absorption for SPH-based DualSPHysics model. *Coastal Engineering*, 127, 37–54. https://doi.org/10.1016/j.coastaleng.2017.06.004
[8] Verbrugghe, T., Domínguez, J.M., Altomare, C., Tafuni, A., Vacondio, R., Troch, P., Kortenhaus, A., 2019. Nonlinear wave generation and absorption using open boundaries within DualSPHysics. *Computer Physics Communication*, 240, 46–59. https://doi.org/10.1016/j.cpc.2019.02.003
[9] Chow, A.D., Rogers, B.D., Lind, S.J., Stansby, P.K., 2019. Numerical wave basin using incompressible smoothed particle hydrodynamics (ISPH) on a single GPU with vertical cylinder test cases. *Computer and Fluids*, 179, 543–562. https://doi.org/10.1016/j.compfluid.2018.11.022
[10] Syamsuri, Chern, M.-J., Vaziri, N., 2020. SPH model for interaction of sloshing wave with obstacle in shallow water tank. *Journal of King Saud University Engineering Science*, 34, 2, 126-138. https://doi.org/10.1016/j.jksues.2020.07.009
[11] Trimulyono, A., Samuel, Iqbal, M., 2020. Sloshing Simulation of Single-Phase and Two-Phase SPH using DualSPHysics. *Kapal: Jurnal Ilmu Pengetahuan dan Teknologi Kelautan*, 17, 50–57. https://doi.org/10.14710/kapal.v17i2.27892
[12] Trimulyono, A., Chrismianto, D., Samuel, S., Aslami, M.H., 2021. Single-phase and two-phase smoothed particle hydrodynamics for sloshing in the low filling ratio of the prismatic tank. *International Journal of Engineering, Transactions B: Applications*, 34, 1345–1351. https://doi.org/10.5829/ije.2021.34.05b.30
[13] Hu, T., Wang, S., Zhang, G., Sun, Z., Zhou, B., 2019. Numerical simulations of sloshing flows with an elastic baffle using a SPH-SPIM coupled method. *Applied Ocean Research*, 93, 101950. https://doi.org/10.1016/j.apor.2019.101950
[14] Ünal, U.O., Bilici, G., Akyıldız, H., 2019. Liquid sloshing in a two-dimensional rectangular tank: A numerical investigation with a T-shaped baffle. *Ocean Engineering*, 187, 106183. https://doi.org/10.1016/j.oceaneng.2019.106183
[15] Zhang, Z.L., Khalid, M.S.U., Long, T., Chang, J.Z., Liu, M.B., 2020. Investigations on sloshing mitigation using elastic baffles by coupling smoothed finite element method and decoupled finite particle method. *Journal of Fluids and Structures*, 94, 102942. https://doi.org/10.1016/j.jfluidstructs.2020.102942
[16] Green, M.D., Zhou, Y., Dominguez, J.M., Gesteira, M.G., Peiró, J., 2021. Smooth particle hydrodynamics simulations of long-duration violent three-dimensional sloshing in tanks. *Ocean Engineering*, 229, 108925. https://doi.org/10.1016/j.oceaneng.2021.108925
[17] Zhang, Z.L., Khalid, M.S.U., Long, T., Liu, M.B., Shu, C., 2021. Improved element-particle coupling strategy with δ-SPH and particle shifting for modeling sloshing with rigid or deformable structures. *Applied Ocean Research*, 114, 102774. https://doi.org/10.1016/j.apor.2021.102774
[18] Cai, Z., Topa, A., Djukic, L.P., Herath, M.T., Pearce, G.M.K., 2021. Evaluation of rigid body force in liquid sloshing problems of a partially filled tank: Traditional CFD/SPH/ALE comparative study. *Ocean Engineering*, 236, 109556. https://doi.org/10.1016/j.oceaneng.2021.109556
[19] Ma, C., Xiong, C., Ma, G., 2021. Numerical study on suppressing violent transient sloshing with single and double vertical baffles. *Ocean Engineering*, 223, 108557. https://doi.org/10.1016/j.oceaneng.2020.108557
[20] Trimulyono, A., Hashimoto, H., Matsuda, A., 2019. Experimental validation of single- and two-phase smoothed particle hydrodynamics on sloshing in a prismatic tank. *Journal Marine Science and Engineering*, 7(8), 247. https://doi.org/10.3390/jmse7080247
[21] Domínguez, J.M., Fourtakas, G., Altomare, C., Canelas, R.B., Tafuni, A., García-Feal, O., Martínez-Estévez, I., Mokos, A., Vacondio, R., Crespo, A.J.C., Rogers, B.D., Stansby, P.K., Gómez-Gesteira, M., 2021. DualSPHysics: from fluid dynamics to multiphysics problems. *Computational Particle Mechanics*. https://doi.org/10.1007/s40571-021-00404-2
[22] Domínguez, J.M., Crespo, A.J.C., Gómez-Gesteira, M., 2013. Optimization strategies for CPU and GPU implementations of a smoothed particle hydrodynamics method. *Computer Physics Communications*, 184, 617–627. https://doi.org/10.1016/j.cpc.2012.10.015
[23] L. B. Lucy, 1977. A numerical approach to the testing of the fission hypothesis. *Astronomical Journal*, 82, 1013–1024. https://doi.org/10.1086/112164
[24] Liu, G.-R., Liu, M.B., 2003. Smoothed Particle Hydrodynamics: A Meshfree Particle Method, World Scientific. *World Scientific*. https://doi.org/10.1142/9789812564405
[25] Violeau, D., 2012. Fluid Mechanics and the SPH Method: Theory and Applications. OUP Oxford. https://doi.org/10.1093/acprof:oso/9780199655526.001.0001

[26] Molteni, D., Colagrossi, A., 2009. A simple procedure to improve the pressure evaluation in hydrodynamic context using the SPH. *Computer Physics Communications*, 180, 861–872. https://doi.org/10.1016/j.cpc.2008.12.004
[27] Pringgana, G., 2015. Improving resilience of coastal structures subject to tsunami-like waves. PhD Thesis. University of Manchester, UK.
[28] Crespo, A.J.C., Gómez-Gesteira, M., Dalrymple, R.A. 2007. Boundary conditions generated by dynamic particles in SPH methods. *Computers, Materials & Continua*, 5, 173-184.
[29] García-Feal, O., Crespo, A.J.C., Gómez-Gesteira, M., 2021. VisualSPHysics: advanced fluid visualization for SPH models. *Computational Particle Mechanics*. https://doi.org/10.1007/s40571-020-00386-7

Submitted: 11.11.2021.
Accepted: 11.04.2022.

Andi Trimulyono
Assistant Professor, Department of Naval Architecture, Universitas Diponegoro, Semarang, Indonesia (anditrimulyono@live.undip.ac.id)
Haikal Atthariq
Research scholar, Department of Naval Architecture, Universitas Diponegoro, Semarang, Indonesia
Deddy Chrismianto
Assistant Professor, Department of Naval Architecture, Universitas Diponegoro, Semarang, Indonesia
S Samuel
Assistant Professor , Department of Naval Architecture, Universitas Diponegoro, Semarang, Indonesia